Defect-assisted nonradiative recombination in $Cu_2ZnSnSe_4$: A comparative study with Cu_2ZnSnS_4

Yonggang Xu,[1] Ji-Hui Yang,[1] Shiyou Chen,[2] and Xin-Gao Gong[1,3]

[1]*Key Laboratory for Computational Physical Sciences (MOE), State Key Laboratory of Surface Physics, Department of Physics, Fudan University, Shanghai 200433, China*

[2]*Key Laboratory of Polar Materials and Devices (MOE) and Department of Electronics, East China Normal University, Shanghai 200241, China*

[3]*Collaborative Innovation Center of Advanced Microstructures, Nanjing, 210093, China*

(Received 12 June 2020; accepted 9 December 2020; published 15 February 2021)

The efficiencies of $Cu_2ZnSnSe_4$ (CZTSe) solar cells with a narrower band gap at 1.0 eV are currently higher than those of Cu_2ZnSnS_4 (CZTS), with the optimal band gap according to the Shockley-Queisser model. To understand this abnormal observation, we studied the nonradiative recombination rates induced by the deep levels of the dominant defects in CZTSe, i.e., the $Sn_{Zn}(2+/+)$, $Sn_{Zn}(+/0)$, and $[Cu_{Zn}\text{-}Sn_{Zn}](+/0)$ levels. We found that the effective recombination centers in CZTS, namely, Sn_{Zn}^{2+} and $[Cu_{Zn}\text{-}Sn_{Zn}]^{+}$, have much smaller carrier capture rates in CZTSe, and are less detrimental to the minority carrier lifetime and energy conversion efficiency. The smaller carrier capture rates for CZTSe can be attributed to the higher electronic transition energies, lower phonon frequencies, and weaker electron-phonon coupling effects in CZTSe compared to those in CZTS, because the large Se cations give rise to larger lattice constants and a softer lattice in CZTSe.

DOI: 10.1103/PhysRevMaterials.5.025403

I. INTRODUCTION

Kesterite quaternary compounds Cu_2ZnSnS_4 (CZTS) and $Cu_2ZnSnSe_4$ (CZTSe) have become the subjects of intensive interest as promising thin-film solar cell light-absorber semiconductors, because of their optimal band gaps [1–6], remarkable absorption coefficients ($>10^4 cm^{-1}$) [7], abundant and nontoxic elemental components, and growth techniques compatible with the commercialized thin-film solar cells such as $Cu(In, Ga)Se_2$ [8] cells. According to Shockley-Queisser theory [6], the maximum energy conversion efficiency of CZTS and CZTSe with band gaps of 1.5 and 1.0 eV are 32.4 and 31%, respectively, so CZTS solar cells should have higher efficiency than CZTSe cells. However, the efficiency of CZTS solar cells achieved experimentally stagnated at around 9% [9,10] and only recently reached 11% [11]. For CZTSe solar cells, the achieved efficiency is slightly higher, at 11.6% [12]. So far, the record photovoltaic efficiency of the thin-film solar cells based on the alloys of CZTS and CZTSe is still 12.6%, which was reported in 2013. These efficiencies are still far below their theoretical limits (around 32%) [6,13,14].

To understand the efficiency-limiting factors, comparative studies on CZTS and CZTSe can provide useful information. In recent years it has been observed that CZTS, with an optimal band gap of 1.5 eV, has a lower efficiency than CZTSe, with a much narrower band gap, and this unexpected phenomenon has been studied from different perspectives, such as using a Mo back contact, and considering the doping ability of the isolated bulk materials [15–17]. However, the microscopic origin is still under debate and remains open.

Among the efficiency-limiting factors, the minority carrier lifetime plays an important role. The measured minority carrier lifetime of CZTS is several nanoseconds [8,18,19], much shorter than the typical lifetime for high-efficiency $Cu(In, Ga)Se_2$ [20,21], at tens to hundreds of nanoseconds. The shorter carrier lifetime is usually attributed to the nonradiative recombination induced by deep-level defects, which is often described by the Shockley-Read-Hall (SRH) model [16,18,19,22–27]. Consequently, it will be important to understand the impacts of deep-level defects on carrier lifetime and photovoltaic conversion efficiency in CZTS and CZTSe. However, it is difficult both experimentally and theoretically to identify the effective nonradiative center defects. In experiment, a large number of defects produce various defect levels in the band gap, making it hard to specify the role of a specific defect [28–30]. In theory, multiphonon-assisted electronic transition requires special treatment, such as nonadiabatic description, or static coupling theory treatment. The computational formalism of static coupling theory treatment was derived very recently, and the result is proved to be consistent with experiments [31,32]. It is very difficult to predict the effects of a large number of point defects on the nonradiative recombination before the multiphonon-assisted electronic transition rates can be calculated using this formalism.

In this work, using static coupling formalism and considering the electron-phonon coupling effect, we have quantitatively calculated the nonradiative carrier recombination rates of the dominant deep-level defects, which are Sn_{Zn} antisites and Cu_{Zn}-Sn_{Zn} clusters. We find that Sn_{Zn}^{2+} and $[Cu_{Zn}\text{-}Sn_{Zn}]^{+}$ in CZTSe have much smaller recombination rates compared to those in CZTS, which can explain the higher efficiency of CZTSe cells. From chemical trends analysis of the main factors that affect nonradiative recombination rate from CZTS to CZTSe, we find that the higher

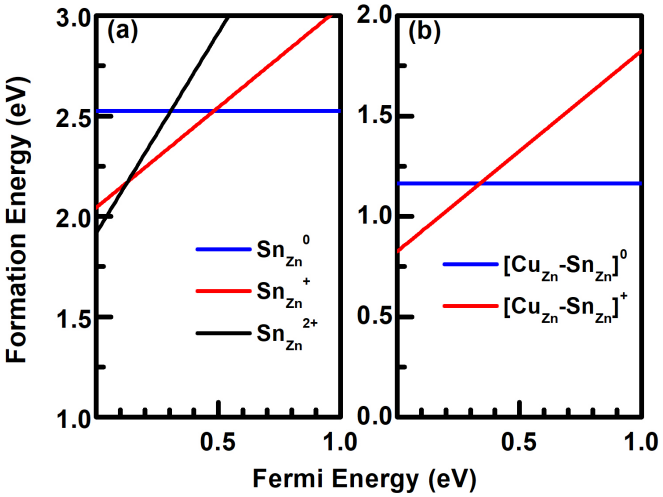

FIG. 1. Calculated defect formation energies as a function of Fermi level. (a) Formation energies of neutral, +1, and +2 charge states are plotted for Sn_{Zn} antisite, and (b) formation energies of neutral and +1 charge states are plotted for Cu_{Zn}-Sn_{Zn} antisite clusters. The Fermi energy is referenced to the VBM level and the chemical potentials $\mu_{Zn} = -1.23$ eV, $\mu_{Cu} = -0.20$ eV, and $\mu_{Sn} = -0.50$ eV are applied. The Fermi energy at which formation energies cross is defined as the defect transition level.

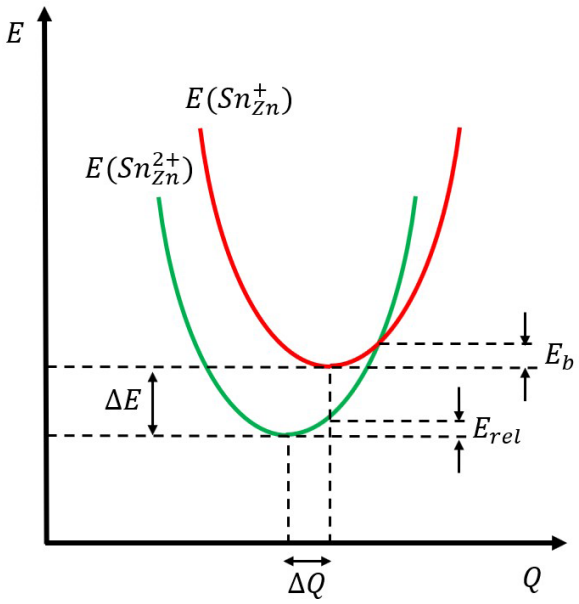

FIG. 2. 1D configuration diagram of the nonradiative $Sn_{Zn}(2+/+)$ transition under the harmonic approximation. The green parabola refers to the initial state (+2 charged Sn_{Zn} state) and the red parabola refers to the final state (+1 charged Sn_{Zn} state). Q denotes the generalized coordinates of real space, E denotes the total energies, ΔE denotes the electronic transition energy, E_{rel} denotes the relaxation energy, and E_b denotes the transition energy barrier. The nonradiative electronic transition mainly occurs at the cross point of the two energy curves, and the initial system (Sn_{Zn}^{2+}) needs to overcome the energy barrier E_b with the help of thermal excitations.

electronic transition energy, lower phonon energy, and weaker electron-phonon coupling effect in CZTSe are the critical factors that limit the nonradiative recombination rates of Sn_{Zn}^{2+} and $[Cu_{Zn}\text{-}Sn_{Zn}]^{+}$ defects. These factors are corelated with the larger lattice constants and softer lattice of CZTSe compared to CZTS.

II. CALCULATION METHOD

The formation energy of a defect determines its equilibrium density in the lattice. In the supercell model, the defect formation energy is calculated according to $\Delta H(\alpha) = E(\alpha) - E(host) + \sum_i n_i(E_i + \mu_i)$, where $E(\alpha)$ and $E(host)$ are the total energies of the supercell with a defect α and without defect, respectively. E_i refers to the total energy of the element i in its pure phase and n_i is the number of i atoms removed from the supercell in the process of defect formation. Negative n_i indicates introduction of element i to the supercell. The calculated formation energies of Sn_{Zn} and Cu_{Zn}-Sn_{Zn} defects as a function of Fermi energy are plotted as shown in Fig. 1. The formation energies of the positively charged defects, namely Sn_{Zn}^{2+}, Sn_{Zn}^{+} [Fig. 1(a)] and $[Cu_{Zn}\text{-}Sn_{Zn}]^{+}$ [Fig. 1(b)], increase when the Fermi energy shifts up from the valence-band maximum (VBM) to the conduction-band minimum (CBM). The Fermi energy at which the formation energy lines intersect is defined as the defect transition energy level [denoted as $Sn_{Zn}(2+/+)$ for example].

A defect level in the band gap can induce a nonradiative recombination by capturing an electron from the CBM state and a hole from the VBM state, releasing energy through phonon excitations. The nonradiative recombination rate is directly determined by the electron and hole capture rates of the defect level. In synthesized CZTS(Se), intrinsic p-type conductivity is widely observed, while n-type samples have not yet been reported [27,33–35]. Density-functional theory calculations suggest that in CZTS(Se), the formation energies of most acceptor defects are lower than those of donor defects. Thus, the high population of acceptors (Cu_{Zn} antisite and Cu vacancy) determines the intrinsic p-type conductivity of CZTS(Se) [16,26]. As a result, in both CZTS and CZTSe, the concentration of hole carriers is enormously larger than that of electron carriers. Electrons are minority carriers and the hole capture time is negligible compared to the electron capture time. Consequently, in this work, we have calculated the electron capture coefficient to approximate the nonradiative recombination rates.

Static coupling formalism is used to describe the nonradiative carrier capture process [31,36,37] and the Sommerfeld factor f_s is applied to describe the attractive Coulomb interaction of the electron and the positively charged centers [38]. The final electron capture coefficient is given by $B_e = f_s\tilde{B}_e$, where $\tilde{B}_e$ is the calculated electron capture coefficient given by static coupling formalism [39].

To analyze the physical origins of the difference in the calculated nonradiative recombination rates between CZTSe and CZTS, the calculations of the transition energy barrier E_b, electronic transition energy ΔE, and lattice relaxation energy E_{rel} are performed. Under the harmonic approximation, the nonradiative electronic transition can be described by the one-dimensional configuration diagram, as shown in Fig. 2. The nonradiative electronic transition mainly occurs

at the intersection of the energy curves; the initial system needs to overcome the energy barrier denoted as E_b in Fig. 2. Hence, the electronic capture coefficient is sensitive to the transition energy barrier and it is reported that the relation between the electronic capture coefficient and the transition energy barrier is well fitted with $B_e = B_0 + B_1 \exp(-\frac{E_b}{k_b T})$ [40]. Following the harmonic approximation, the transition energy barrier depends on the electronic transition energy ΔE and lattice relaxation energy $E_{\rm rel}$, by $E_b = \frac{(\Delta E - E_{\rm rel})^2}{4E_{\rm rel}}$ [36,37], where $E_{\rm rel} = \sum_k \frac{1}{2}\omega_k^2 \Delta Q_k^2$ [41,42], ω_k is the phonon frequency, and ΔQ_k is the coordination difference between the initial and final states projected on each phonon mode k.

In all the calculations, 64-atom supercells of kesterite CZTSe and CZTS are used [43,44]. The Heyd-Scuseria-Ernzerhof hybrid functional, with 25% of the Perdew-Burke-Ernzerhof exchange functional [45,46] replaced by the screened Hartree-Fock exchange, is adopted to correct the band gaps, and the screening parameter is set to 0.2 Å^{-1}. The Vienna *Ab initio* Simulation Package (VASP) [47] with the projected augmented-wave pseudopotentials [48] is used to perform the structural relaxation and calculate the phonon spectrum. The cutoff energy of the plane-wave basis is 400 eV and the atomic structures are relaxed until the atomic forces are smaller than 0.01 eV Å^{-1}. The electron-phonon coupling matrices are calculated using QUANTUM ESPRESSO [49] with the finite-difference method, in which the norm-conserving pseudopotentials and a cutoff energy of 90 Ry for the plane-wave basis are applied. Finite-size effect correction and potential alignment are implicitly included for the charged defects [50].

III. RESULTS AND DISCUSSION

In CZTSe and CZTS, the Sn_{Zn} antisite defect and Cu_{Zn}-Sn_{Zn} defect clusters can have high concentrations [16,25,27,51–54] and act as possible nonradiative recombination centers limiting the minority carrier lifetime. As a donor defect, a Sn_{Zn} antisite can have three charge states, namely, 0 (neutral, not ionized), +1, and +2. Accordingly, the transitions between the three levels produce three transition energy levels in the band gap, i.e., (+/0), (+2/+), and (+2/0). As shown in Fig. 3, the charge density of the defect level induced by the neutral antisite is localized at the defect site. Cu_{Zn}-Sn_{Zn} has two stable charge states, the neutral state and the +1 charged state, and has one transition energy level (+/0). Due to Coulomb repulsion, it is unlikely for a defect to capture two electrons simultaneously. Therefore, we only consider the single-electron (or single-hole) capture process, including electron capture by the (+/0) and (+2/+) levels of Sn_{Zn} and electron capture by the (+/0) level of [Cu_{Zn}-Sn_{Zn}] [55,56].

In CZTS, our previous study showed that $Sn_{Zn}(2+/+)$, $Sn_{Zn}(+/0)$, and [Cu_{Zn}-Sn_{Zn}](+/0) are all deep levels, which are 0.83, 0.64, and 1.17 eV above VBM, respectively. However, these three transitions show varying electron capture coefficients at 300 K. The electron capture coefficient due to the $Sn_{Zn}(2+/+)$ transition and the [Cu_{Zn}-Sn_{Zn}](+/0) transition are comparable, with the values of 2.4×10^{-6} cm^3/s and 1.2×10^{-6} cm^3/s respectively. In contrast, the electron capture coefficient due to the $Sn_{Zn}(+/0)$ transition is smaller by almost four orders of magnitude, only 1.3×10^{-10} cm^3/s. Consequently, for CZTS, one could conclude that Sn_{Zn}^{2+} and $[Cu_{Zn}\text{-}Sn_{Zn}]^+$ are effective nonradiative recombination centers limiting the carrier lifetime and photovoltaic conversion efficiency. Further analysis indicated that the smaller capture coefficient of Sn_{Zn}^{+} can be attributed to two factors: (i) The energy of the phonon mode involved in the capture process of Sn_{Zn}^{+} is much lower than the modes involved with Sn_{Zn}^{2+} and $[Cu_{Zn}\text{-}Sn_{Zn}]^+$, accounting for the higher energy barrier of the $Sn_{Zn}(+/0)$ transition, and (ii) the Coulomb attractive interaction between the positive charged defect center Sn_{Zn}^{+} and the electron on the CBM level is weaker compared to the case of Sn_{Zn}^{2+} [37].

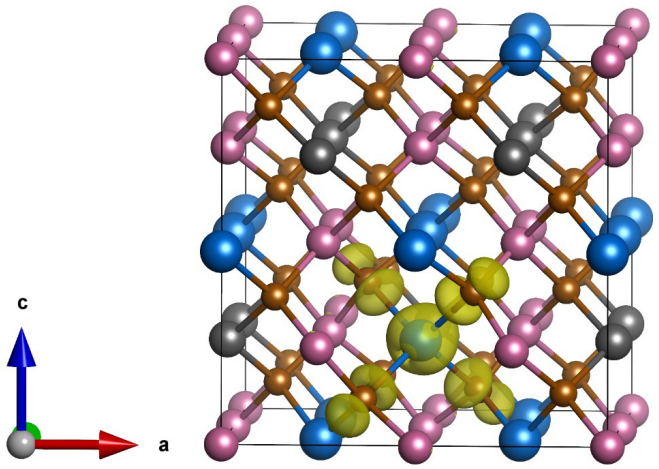

FIG. 3. The charge density of the neutral defect state induced by Sn_{Zn} antisite in CZTSe. The pink, gray, blue, and brown spheres represent Cu, Zn, Sn, and Se atoms, respectively. The defect level induced by Sn_{Zn} antisite is localized at the defect site in the supercell.

For CZTSe, our results in Fig. 1 show that $Sn_{Zn}(+/0)$ and [Cu_{Zn}-Sn_{Zn}](+/0) are also deep levels, 0.48 and 0.34 eV above the VBM, while $Sn_{Zn}(2+/+)$ is only 0.13 eV above the VBM, much lower than that in CZTS (0.83 eV above the VBM). Since the energy difference between the $Sn_{Zn}(2+/+)$ level and the CBM level is up to 0.87 eV in CZTSe, larger than that in CZTS (0.67 eV), the level is close to the VBM and offset from the middle of the band gap. Therefore, we expect that the level is not an effective nonradiative recombination center level according to the SRH model [16]. The calculated electron capture coefficient due to the $Sn_{Zn}(2+/+)$ transition in CZTSe is only $3.5 \times 10^{-9}\text{cm}^3/\text{s}$, three orders of magnitude smaller than that in CZTS, indicating that this level is indeed not important for nonradiative recombination.

In contrast, the $Sn_{Zn}(+/0)$ and [Cu_{Zn}-Sn_{Zn}](+/0) levels are deep in the band gap, so we expect that they should cause significant nonradiative recombination according to the SRH model. However, their calculated electron capture coefficients are small, $3.3 \times 10^{-9}\text{cm}^3/\text{s}$ and $6.6 \times 10^{-9}\text{cm}^3/\text{s}$, respectively. As a result, none of these defects is an effective nonradiative recombination center in CZTSe, which is clearly different from the cases in CZTS where the $Sn_{Zn}(+/0)$ and [Cu_{Zn}-Sn_{Zn}](+/0) levels have large electron capture coefficients.

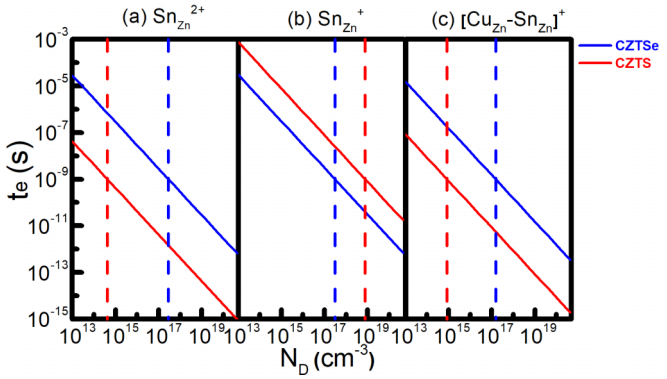

FIG. 4. Dependences of the maximal SRH recombination lifetimes of minority carriers (electrons) on the concentrations of Sn_{Zn}^{2+} (a), Sn_{Zn}^{+} (b), and $[Cu_{Zn}\text{-}Sn_{Zn}]^{+}$ (c) in CZTSe (blue lines), respectively. The lifetime dependences on defect concentration in CZTS (red lines) are also plotted for comparison. The dashed lines show the concentration of defects above which the minority carrier lifetime is limited below 1 ns.

Using the calculated electron capture coefficients, denoted as B_e above, we estimate the effects of the aforementioned defects on the SRH recombination minority carrier lifetimes τ_{SRH}, which are given by $\tau_{\mathrm{SRH}} = \frac{1}{B_e N_d}$ with N_d being the defect concentration. As shown in Fig. 4, if the concentration is as high as $10^{15}\mathrm{cm}^{-3}$, the defects Sn_{Zn}^{2+}, Sn_{Zn}^{+}, and $[Cu_{Zn}\text{-}Sn_{Zn}]^{+}$ will limit the carrier (electron) lifetime to be 0.4 ns, 8 μs, 0.8 ns, respectively, in CZTS and 0.3, 0.3, 0.2 μ s, respectively, in CZTSe. For comparisons, typical experimentally measured carrier lifetime is on the nanosecond scale [8,18,19]. If the carrier lifetime needs to be longer than $\sim$1 ns, the concentrations of Sn_{Zn}^{2+} and $[Cu_{Zn}\text{-}Sn_{Zn}]^{+}$ should be lower than 4.2×10^{14} cm^{-3}, 8.3×10^{14} cm^{-3}, respectively, in CZTS, and $2.9 \times 10^{17}\mathrm{cm}^{-3}$, $1.5 \times 10^{17}\mathrm{cm}^{-3}$ respectively in CZTSe, (see the dashed lines in Fig. 4). Obviously, Sn_{Zn}^{2+} and $[Cu_{Zn}\text{-}Sn_{Zn}]^{+}$ are more detrimental to the carrier lifetime and energy conversion efficiency in CZTS than CZTSe, explaining the better efficiency of CZTSe.

The experimentally measured minority carrier lifetime τ depends on all recombination lifetimes including radiative recombination lifetime (τ_R), SRH recombination lifetime (τ_{SRH}), Auger recombination lifetime (τ_A), and surface recombination lifetime (τ_{Surf}), which can be formulized as

$$\frac{1}{\tau} = \frac{1}{\tau_R} + \frac{1}{\tau_{\mathrm{SRH}}} + \frac{1}{\tau_A} + \frac{1}{\tau_{\mathrm{Surf}}}.$$

Our calculations only include the SRH recombination lifetime. The experimentally measured minority carrier lifetimes of CZTS are all around several nanoseconds [12,57–59], which are on the order of the calculated SRH recombination lifetime. Thus, we conclude that in CZTS, the SRH recombination is one of the dominant factors that limit the minority carrier lifetime. However, for CZTSe, the experimentally measured minority carrier lifetimes are also around several nanoseconds [12,60,61], which are much smaller than the calculated SRH recombination lifetimes. We infer that, for CZTSe, the interface and surface recombination rather than the SRH recombination limits the minority carrier lifetime dominantly. Experimentally, Barkhouse *et al.* have proposed that their record CZTSSe device is primarily limited by the interface recombination [62].

As isovalent semiconductors, CZTSe and CZTS adopt the same crystal structure and share similar electronic and optical properties. Consequently, it is of fundamental interest to understand the significant difference in the calculated electron capture coefficients of the Sn_{Zn}^{2+} and $[Cu_{Zn}\text{-}Sn_{Zn}]^{+}$ defects. In the static coupling formalism, there are four main factors affecting the electron capture coefficients, including the electronic transition energy ΔE, the phonon frequency ω, the lattice distortion ΔQ, and the strength of electron-phonon coupling effect. In the following, we will consider the $Sn_{Zn}(2+/+)$ transition as an example to discuss the differences in these factors between CZTS and CZTSe. The case of the $[Cu_{Zn}\text{-}Sn_{Zn}](+/0)$ transition follows the same way.

A. The electronic transition energy

The electronic transition energy ΔE is defined as the energy difference between the initial and the final states, as shown in Fig. 1. For Sn_{Zn}^{2+}, the electronic transition energy is equal to the defect transition energy level $\varepsilon(+2/+)$ referenced to the CBM level. During the electronic transition, ΔE is always higher than the relaxation energy, so the energy barrier increases as ΔE increases according to $E_b = \frac{(\Delta E - E_{\mathrm{rel}})^2}{4E_{\mathrm{rel}}}$. Specifically, the calculated electronic transition energy of $Sn_{Zn}(2+/+)$ is 0.67 eV for CZTS and is 0.87 eV for CZTSe. As a result, the higher electronic transition energy in CZTSe leads to a higher energy barrier compared to CZTS. We can understand the higher electronic transition energy for CZTSe from two perspectives. On one hand, the antisite Sn atom is surrounded by four S or Se atoms, so the weaker electronegativity of Se atom makes the Coulomb repulsion between the captured electron of a Sn atom and the valence electrons of Se stronger than that in CZTS. On the other hand, the defect level for the Sn_{Zn} antisite is occupied by the p electrons of the Sn atom, which is strongly coupled with the d electrons of the VBM level, and the p-d coupling effect is weaker in CZTSe because the Se atom is larger than the S atom. Consequently, the electronic transition energy in CZTSe is higher than CZTS, resulting in a higher transition barrier and a lower electron capture coefficient in CZTSe.

B. Phonon energy

The nonradiative electronic transition accompanies the multiphonon excitation process. To understand the processes of the electronic transition, we plotted the phonon density of states (DOS) in Fig. 5 and the phonon mode decompositions of Huang-Rhys factors S_k, electron-phonon coupling matrix elements, electronic capture coefficients in Fig. 6, for both CZTSe and CZTS. For CZTS the phonon energy ranges from 0 to 50 meV. Because a Se atom is much heavier than a S atom, the maximal phonon energy of CZTSe is only 32 meV, much lower than the maximal phonon energy of CZTS (47 meV). In addition, the phonon mode decompositions, as well as the projected phonon DOS, which illuminates the phonon contributions from different elements, show different phonon properties of CZTS and CZTSe. For CZTS,

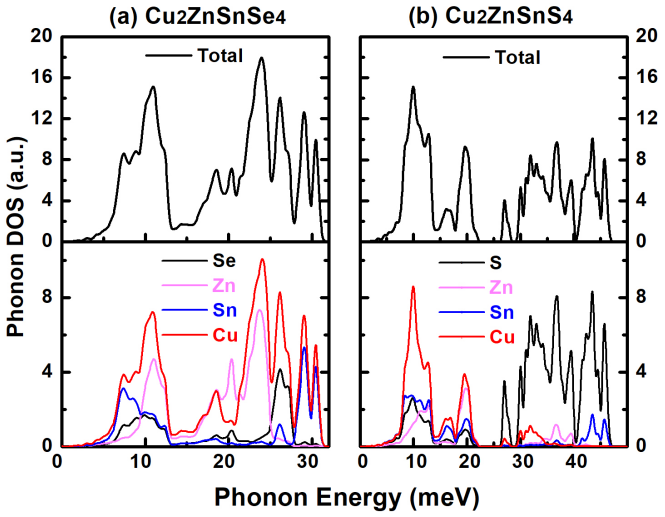

FIG. 5. Total (upper panel) and projected (lower panel) phonon DOS of the 64-atom supercell with a Sn_{Zn}^{2+} antisite defect. (a) The left column is for CZTSe and (b) the right column is for CZTS.

the high-frequency phonon modes are dominated by the vibration of S atoms due to their low mass compared to the heavier Cu, Zn, and Sn atoms, and phonon mode decomposition indicates that the only phonon frequency involved in the nonradiative processes is the vibration of S atoms, mainly the S atoms around the Sn_{Zn}^{2+} defects. In contrast, for CZTSe, the mass difference of the four elements is not significant, so all four elements contribute to both the high-energy part and the low-energy part of the DOS. The phonon mode decomposition also shows that the vibration of all four elements

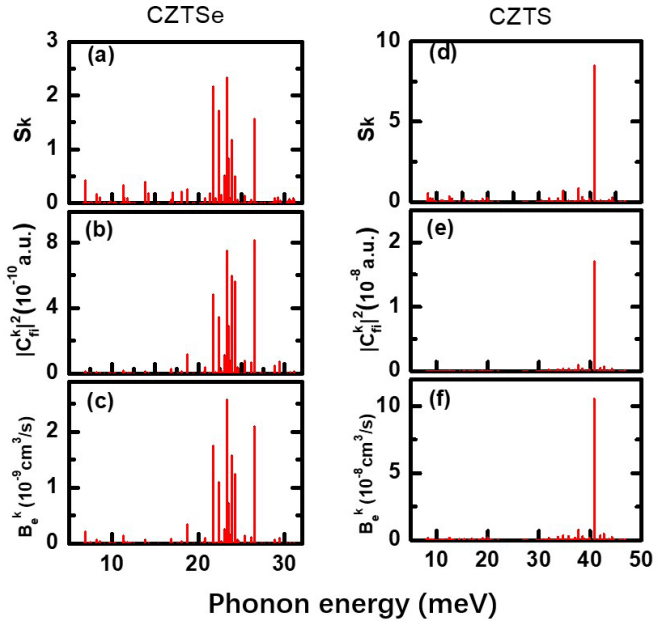

FIG. 6. The contribution of different phonon modes to the (a), (d) Huang-Rhys factor S_k, (b), (e) squared norms of the electron-phonon coupling matrix elements $|C_{fi}^k|^2$, and (c), (f) electron capture coefficient B_e^k at 300 K for the supercell with an antisite Sn_{Zn}^{2+}. The left column is for CZTSe, and the right column is for CZTS.

TABLE I. Sn-Se bond lengths, electronic transition energies ΔE (referenced to CBM level), lattice relaxation energies E_{rel}, and electronic energy barriers E_b for Sn_{Zn}^{2+} defects in CZTSe and CZTS.

Defects	Host	Bond length (Å)	ΔE (eV)	E_{rel} (eV)	$E_b(eV)$
Sn_{Zn}^{2+}	CZTSe	2.58	0.87	0.34	0.21
	CZTS	2.43	0.67	0.50	0.01
$[Cu_{Zn}\text{-}Sn_{Zn}]^{+}$	CZTSe	2.57	0.66	0.29	0.12
	CZTS	2.43	0.33	0.52	0.02

contributes to the electronic transition process. Because the relaxation energy depends on the phonon energy, following $E_{rel} = \sum_k \frac{1}{2}\omega_k^2 \Delta Q_k^2 = \sum_k S_k \hbar\omega_k$, the phonon energy differences make the relaxation energy lower in CZTSe than in CZTS. The calculated relaxation energies support our analysis, i.e., the relaxation energy in CZTSe is only 0.34 eV, while that in CZTS is 0.50 eV, as shown in Table I. The lower relaxation energy results in the higher transition energy barrier in CZTSe, which is one of the most important factors accounting for the lower electron capture coefficients in CZTSe.

C. Lattice distortion

We also compared the difference in lattice distortion during the electronic transition between CZTS and CZTSe semiquantitatively. The lattice distortions are measured by the length changes of the bonds surrounding the defects, namely, the Sn-S bonds for CZTS and Sn-Se bonds for CZTSe. The calculated results show that the defect bond length changes during the $Sn_{Zn}(2+/+)$ transition are 0.14 and 0.12 Å for CZTS and CZTSe, respectively, presenting no significant difference. In other words, the lattice distortion during the $Sn_{Zn}(2+/+)$ transition in CZTS and CZTSe are both very large. However, the electron capture coefficients are significantly different. The low electron capture coefficient of $[Cu_{Zn}\text{-}Sn_{Zn}](+/0)$ in CZTSe demonstrates that a deep-level defect with considerable lattice distortion during the transition process is not necessarily an effective recombination center with a large carrier capture coefficient. More precisely, to be an effective recombination center, the defect should also be surrounded by strong chemical bonds (high-frequency mode) as we proposed in previous work [37]. In CZTSe, the length of the Sn-Se bond in Sn_{Zn}^{2+} is 2.58 Å, longer and softer than the Sn-S bond, with a length of 2.43 Å, in CZTS. The exact and complete empirical criterion for the effective recombination center defects is that the defects surrounded with stronger bonds are more likely to be effective recombination centers.

D. Electron-phonon coupling effect

For the single-electron capture process, i.e., the $Sn_{Zn}(2+/+)$ transition, the electron transits from the CBM level to the defect level. The initial electronic state (the CBM state) and the final electronic state (the defect state) are coupled by all the phonon modes that are plotted in Fig. 6. In static coupling formalism, the electron-phonon coupling matrix is $\langle\psi_f|\frac{\partial H}{\partial Q_k}|\psi_i\rangle$ (denoted as C_{fi}^k) [31,32,36], where the indices i and f denote the initial and final electronic states, respectively, and index k denotes the phonon modes. The

phonon mode decompositions of $|C_{fi}^{k}|^2$ show that a single phonon mode with energy of 41 meV makes the leading contribution to $|C_{fi}^{k}|^2$ ($\sim 10^{-8}$ a.u.) in CZTS; however, the contributions of the leading phonon modes are about two orders of magnitude smaller ($\sim 10^{-10}$ a.u.) in CZTSe. Therefore, the electron-phonon coupling effect for the electronic transition in CZTSe is weaker than that in CZTS, which greatly decreases the electron capture coefficient of the $Sn_{Zn}(2+/+)$ transition for CZTSe. In CZTS, the dominant phonon mode is localized around the Sn_{Zn} defect, where the wave function of the defect electronic state is also localized, so the overlap of the phonon and the electronic state is very large, resulting in strong electron-phonon coupling. However, in CZTSe, many phonon modes contribute to $|C_{fi}^{k}|^2$ and most of these modes are delocalized. Although the electronic state is still localized around the defect, the overall overlap of the phonon and electronic wave function is small, so the electron-phonon coupling is weaker in CZTSe.

IV. CONCLUSION

Using static coupling formalism, we calculated the electron capture coefficients of the $Sn_{Zn}(2+/+)$, $Sn_{Zn}(+/0)$, and $[Cu_{Zn}\text{-}Sn_{Zn}](+/0)$ levels in the band gap of CZTSe. We found that for CZTSe the electron capture coefficients of Sn_{Zn}^{2+} and $[Cu_{Zn}\text{-}Sn_{Zn}]^{+}$ are about three orders of magnitude smaller than those of CZTS, so none of the Sn_{Zn}^{2+}, Sn_{Zn}^{+}, and $[Cu_{Zn}\text{-}Sn_{Zn}]^{+}$ defects in CZTSe is an effective nonradiative recombination center that can seriously limit the carrier lifetime in photovoltaic cells. According to the large difference in the effects of deep-level defects on the minority carrier lifetime, we can understand the higher efficiency achieved in the CZTSe solar cells than in the CZTS cells which have more optimal band gaps. The lower electron capture coefficients of the deep-level defects in CZTSe are attributed to the larger electronic transition energies, lower phonon frequencies (due to the larger lattice constants and softer lattice), and weaker electron-phonon coupling, which lead to higher electronic transition barriers in CZTSe than in CZTS.

ACKNOWLEDGMENTS

This work is supported by the National Key Research and Development Program of China (Grant No. 2016YFB0700700), the National Nature Science Foundation of China (NSFC), and the Supercomputer Center of Fudan University. J.-H.Y. is supported by the Shanghai Sailing Program (Grant No. 19YF1403100). S.C. is supported by the NSFC under Grants No. 61722402 and No. 91833302, and Shanghai Academic/Technology Research Leader (Grant No. 19XD1421300).

[1] X. Liu, Y. Feng, H. Cui, F. Liu, X. Hao, G. Conibeer, D.B. Mitzi, and M. Green, The current status and future prospects of kesterite solar cells: A brief review, Prog. Photovoltaics **24**, 879 (2016).

[2] A. Redinger, D.M. Berg, P. J. Dale, R. Djemour, L. Guetay, T. Eisenbarth, N. Valle, and S. Siebentritt, Route toward high-efficiency single-phase $Cu_2ZnSn(S,Se)(4)$ thin-film solar cells: Model experiments and literature review, IEEE J. Photovoltaics **1**, 200 (2011).

[3] H. Katagiri, T. Washio, H. Shinohara, T. Kurumadani, and S. Miyajima, Development of thin film solar cell based on Cu_2ZnSnS_4 thin films, Sol. Energy Mater. Sol. Cells **65**, 141 (2001).

[4] J. S. Seol, S. Y. Lee, J. C. Lee, H. D. Nam, and K. H. Kim, Electrical and optical properties of Cu_2ZnSnS_4 thin films prepared by rf magnetron sputtering process, Sol. Energy Mater. Sol. Cells **75**, 155 (2003).

[5] N. Kamoun, H. Bouzouita, and B. Rezig, Fabrication and characterization of Cu_2ZnSnS_4 thin films deposited by spray pyrolysis technique, Thin Solid Films **515**, 5949 (2007).

[6] W. Shockley and H. J. Queisser, Detailed balance limit of efficiency of p-n junction solar cells, J. Appl. Phys. **32**, 510 (1961).

[7] K. Ito and T. Nakazawa, Electrical and optical-properties of stannite-type quaternary semiconductor thin-films, Jpn. J. Appl. Phys. Part 1 **27**, 2094 (1988).

[8] I. Repins *et al.*, Co-evaporated $Cu_2ZnSnSe_4$ $Cu_2ZnSnSe_4$ films and devices, Sol. Energy Mater. Sol. Cells **101**, 154 (2012).

[9] B. Shin, O. Gunawan, Y. Zhu, N. A. Bojarczuk, S. J. Chey, and S. Guha, Thin film solar cell with 8.4% power conversion efficiency using an earth-abundant Cu_2ZnSnS_4 absorber, Prog. Photovoltaics Res. Appl. **21**, 72 (2013).

[10] S. Tajima, M. Umehara, M. Hasegawa, T. Mise, and T. Itoh, Cu_2ZnSnS_4 photovoltaic cell with improved efficiency fabricated by high-temperature annealing after CdS buffer-layer deposition, Prog. Photovoltaics Res. Appl. **25**, 14 (2017).

[11] C. Yan *et al.*, Cu_2ZnSnS_4 solar cells with over 10% power conversion efficiency enabled by heterojunction heat treatment, Nat. Energy **3**, 764 (2018).

[12] Y. S. Lee, T. Gershon, O. Gunawan, T. K. Todorov, T. Gokmen, Y. Virgus, and S. Guha, $Cu_2ZnSnSe_4$ thin-film solar cells by thermal co-evaporation with 11.6% efficiency and improved minority carrier diffusion length, Adv. Energy Mater. **5**, 1401372 (2015).

[13] W. Wang, M. T. Winkler, O. Gunawan, T. Gokmen, T. K. Todorov, Y. Zhu, and D. B. Mitzi, Device characteristics of CZTSSe thin-film solar cells with 12.6% efficiency, Adv. Energy Mater. **4**, 1301465 (2014).

[14] S. Kim, J. A. Márquez, T. Unold, and A. Walsh, Upper limit to the photovoltaic efficiency of imperfect crystals from first principles, Energy Environ. Sci. **13**, 1481 (2020).

[15] S. Chen, A. Walsh, J. H. Yang, X. G. Gong, L. Sun, P. X. Yang, J. H. Chu, and S. H. Wei, Compositional dependence of structural and electronic properties of $Cu_2ZnSn(S,Se)(4)$ alloys for thin film solar cells, Phys. Rev. B **83**, 125201 (2011).

[16] S. Chen, A. Walsh, X.-G. Gong, and S.-H. Wei, Classification of lattice defects in the kesterite Cu_2ZnSnS_4 and $Cu_2ZnSnSe_4$ earth-abundant solar cell absorbers, Adv. Mater. **25**, 1522 (2013).

[17] H. J. Gu, J.-H. Yang, S. Y. Chen, H. J. Xiang, and X. G. Gong, Interfacial engineering to improve Cu_2ZnSnX_4 (X = S, Se) solar cell efficiency, APL Mater. **7**, 091104 (2019).

[18] M. Kumar, A. Dubey, N. Adhikari, S. Venkatesan, and Q. Qiao, Strategic review of secondary phases, defects and defect-complexes in kesterite CZTS-Se solar cells, Energy Environ. Sci. **8**, 3134 (2015).

[19] O. Gunawan, T. K. Todorov, and D. B. Mitzi, Loss mechanisms in hydrazine-processed $Cu_2ZnSn(Se,S)(4)$ solar cells, Appl. Phys. Lett. **97**, 233506 (2010).

[20] I. L. Repins, W. K. Metzger, C. L. Perkins, J. V. Li, and M. A. Contreras, Correlation between measured minority-carrier lifetime and Cu(In, Ga)Se-2 device performance, IEEE Trans. Electron Devices **57**, 2957 (2010).

[21] W. K. Metzger, I. L. Repins, M. Romero, P. Dippo, M. Contreras, R. Noufi, and D. Levi, Recombination kinetics and stability in polycrystalline Cu(In,Ga)Se-2 solar cells, Thin Solid Films **517**, 2360 (2009).

[22] W. Shockley and W. T. Read, Statistics of the recombinations of holes and electrons, Phys. Rev. **87**, 835 (1952).

[23] R. N. Hall, Electron-hole recombination in germanium, Phys. Rev. **87**, 387 (1952).

[24] A. Polman, M. Knight, E. C. Garnett, B. Ehrler, and W. C. Sinke, Photovoltaic materials: present efficiencies and future challenges, Science **352**, aad4424 (2016).

[25] D. Han, Y. Y. Sun, J. Bang, Y. Y. Zhang, H. B. Sun, X. B. Li, and S. B. Zhang, Deep electron traps and origin of p-type conductivity in the earth-abundant solar-cell material Cu_2ZnSnS_4, Phys. Rev. B **87**, 155206 (2013).

[26] A. Walsh, S. Chen, S.-H. Wei, and X.-G. Gong, Kesterite thin-film solar cells: Advances in materials modelling of Cu_2ZnSnS_4, Adv. Energy Mater. **2**, 400 (2012).

[27] S. Chen, L.-W. Wang, A. Walsh, X. G. Gong, and S.-H. Wei, Abundance of Cu-Zn + Sn-Zn and 2Cu(Zn) + Sn-Zn defect clusters in kesterite solar cells, Appl. Phys. Lett. **101**, 223901 (2012).

[28] S. Jursenas, S. Miasojedovas, G. Kurilcik, A. Zukauskas, and P. R. Hageman, Luminescence decay in highly excited GaN grown by hydride vapor-phase epitaxy, Appl. Phys. Lett. **83**, 66 (2003).

[29] M. A. Reshchikov, A. A. Kvasov, M. F. Bishop, T. McMullen, A. Usikov, V. Soukhoveev, and V. A. Dmitriev, Tunable and abrupt thermal quenching of photoluminescence in high-resistivity Zn-doped GaN, Phys. Rev. B **84**, 075212 (2011).

[30] T. Tsuchiya, Interactions between interface traps in electron capture/emission processes: Deviation from charge pumping current based on the Shockley-Read-Hall theory, Appl. Phys. Express **4**, 094104 (2011).

[31] L. Shi and L.-W. Wang, Ab initio Calculations of Deep-Level Carrier Nonradiative Recombination Rates in Bulk Semiconductors, Phys. Rev. Lett. **109**, 245501 (2012).

[32] L. Shi, K. Xu, and L. W. Wang, Comparative study of ab initio nonradiative recombination rate calculations under different formalisms, Phys. Rev. B **91**, 205315 (2015).

[33] S. Chen, X. G. Gong, A. Walsh, and S.-H. Wei, Defect physics of the kesterite thin-film solar cell absorber Cu_2ZnSnS_4, Appl. Phys. Lett. **96**, 021902 (2010).

[34] S. Chen, J. H. Yang, X. G. Gong, A. Walsh, and S. H. Wei, Intrinsic point defects and complexes in the quaternary kesterite semiconductor Cu_2ZnSnS_4, Phys. Rev. B **81**, 245204 (2010).

[35] A. Nagoya, R. Asahi, R. Wahl, and G. Kresse, Defect formation and phase stability of Cu_2ZnSnS_4 photovoltaic material, Phys. Rev. B **81**, 113202 (2010).

[36] J. Li, H. F. Zhu, Y. Y. Zhang, Z. K. Yuan, S. Chen, and X. G. Gong, Large carrier-capture rate of Pb-I antisite in $CH_3NH_3PbI_3$ induced by heavy atoms and soft phonon modes, Phys. Rev. B **96**, 104103 (2017).

[37] J. Li, Z.-K. Yuan, S. Chen, X.-G. Gong, and S.-H. Wei, Effective and noneffective recombination center defects in Cu_2ZnSnS_4: Significant difference in carrier capture cross sections, Chem. Mater. **31**, 826 (2019).

[38] R. Passler, Relationships between nonradiative multiphonon carrier-capture properties of deep charged and neutral centers in semiconductors, Phys. Status Solidi B **78**, 625 (1976).

[39] A. Alkauskas, C. E. Dreyer, J. L. Lyons, and C. G. VandeWalle, Role of excited states in Shockley-Read-Hall recombination in wide-band-gap semiconductors, Phys. Rev. B **93**, 201304(R) (2016).

[40] A. Alkauskas, Q. Yan, and C. G. VandeWalle, First-principles theory of nonradiative carrier capture via multiphonon emission, Phys. Rev. B **90**, 075202 (2014).

[41] R. Kubo and Y. Toyozawa, Application of the method of generating function to radiative and non-radiative transitions of a trapped electron in a crystal, Prog. Theor. Phys. **13**, 160 (1955).

[42] K. Huang, Lattice relaxation and multiphonon transitions, Contemp. Phys. **22**, 599 (1981).

[43] J. Heyd, G. E. Scuseria, and M. Ernzerhof, Hybrid functionals based on a screened Coulomb potential, J. Chem. Phys. **118**, 8207 (2003).

[44] J. Heyd, G. E. Scuseria, and M. Ernzerhof, Erratum: "Hybrid functionals based on a screened Coulomb potential" [J. Chem. Phys. 118, 8207 (2003)], J. Chem. Phys. **124**, 219906 (2006).

[45] J. P. Perdew, K. Burke, and M. Ernzerhof, Generalized Gradient Approximation Made Simple, Phys. Rev. Lett. **77**, 3865 (1996).

[46] J. P. Perdew, K. Burke, and M. Ernzerhof, Generalized Gradient Approximation Made Simple [Phys. Rev. Lett. **77**, 3865 (1996)], Phys. Rev. Lett. **78**, 1396(E) (1997).

[47] G. Kresse and J. Furthmuller, Efficient iterative schemes for ab initio total-energy calculations using a plane-wave basis set, Phys. Rev. B **54**, 11169 (1996).

[48] P. E. Blöchl, Projector augmented-wave method, Phys. Rev. B **50**, 17953 (1994).

[49] P. Giannozzi *et al.*, Quantum espresso: A modular and open-source software project for quantum simulations of materials, J. Phys.: Condens. Matter **21**, 395502 (2009).

[50] S. Lany and A. Zunger, Assessment of correction methods for the band-gap problem and for finite-size effects in supercell defect calculations: Case studies for ZnO and GaAs, Phys. Rev. B **78**, 235104 (2008).

[51] K. Biswas, S. Lany, and A. Zunger, The electronic consequences of multivalent elements in inorganic solar absorbers: Multivalency of Sn in Cu_2ZnSnS_4, Appl. Phys. Lett. **96**,201902 (2010).

[52] M. Grossberg, T. Raadik, J. Raudoja, and J. Krustok, Photoluminescence study of defect clusters in Cu_2ZnSnS_4 polycrystals, Curr. Appl Phys. **14**, 447 (2014).

[53] S. Kim, J.-S. Park, and S. N. Hood Lone-pair effect on carrier capture in Cu_2ZnSnS_4 solar cells, J. Mater. Chem. A **7**, 2686 (2019).

[54] S. Kim, J.-S. Park, and A. Walsh, Identification of killer defects in kesterite thin-film solar cells, ACS Energy Lett. **3**, 496 (2018).

[55] S. H. Wei, Overcoming the doping bottleneck in semiconductors, Comput. Mater. Sci. **30**, 337 (2004).

[56] S. B. Zhang, S. H. Wei, A. Zunger, and H. Katayama-Yoshida, Defect physics of the $CuInSe_2$ chalcopyrite semiconductor, Phys. Rev. B **57**, 9642 (1998).

[57] Y. F. Tay *et al.*, Solution-processed Cd-substituted CZTS photocathode for efficient solar hydrogen evolution from neutral water, Joule **2**, 537 (2018).

[58] F. Liu, C. Yan, J. Huang, K. Sun, F. Zhou, J. A. Stride, M. A. Green, and X. Hao, Nanoscale microstructure and chemistry of Cu_2ZnSnS_4/CdS interface in kesterite Cu_2ZnSnS_4 solar cells, Adv. Energy Mater. **6**, 1600706 (2016).

[59] K. Sun, C. Yan, J. Huang, K. Sun, H. Sun, L. Jiang, X. Deng, J. Stride, X. Hao, and F. Liu, Minority lifetime and efficiency improvement for CZTS solar cells via Cd ion soaking and post treatment, J. Alloys Compd. **750**, 328 (2018).

[60] C. J. Hages, M. J. Koeper, and R. Agrawal, Optoelectronic and material properties of nanocrystal-based CZTSe absorbers with Ag-alloying, Sol. Energy Mater. Sol. Cells **145**, 342 (2016).

[61] H. Tampo, K. M. Kim, S. Kim, H. Shibata, and S. Niki, Improvement of minority carrier lifetime and conversion efficiency by Na incorporation in $Cu_2ZnSnSe_4$ solar cells, J. Appl. Phys. **122**, 023106 (2017).

[62] D. A. R. Barkhouse, R. Haight, N. Sakai, H. Hiroi, H. Sugimoto, and D. B. Mitzi, Cd-free buffer layer materials on $Cu_2ZnSn(S_xSe_{1-x})_4$: Band alignments with ZnO, ZnS, and In_2S_3, Appl. Phys. Lett. **100**, 193904 (2012).